Geomechanics and Engineering, *Vol. 30, No. 6 (2022) 489-502*
https://doi.org/10.12989/gae.2022.30.6.489

Meta-heuristic optimization algorithms for prediction of fly-rock in the blasting operation of open-pit mines

Arsalan Mahmoodzadeh[1a], Hamid Reza Nejati*[1], Mokhtar Mohammadi[2b], Hawkar Hashim Ibrahim[3c], Shima Rashidi[4d] and Adil Hussein Mohammed[5e]

[1]*Rock Mechanics Division, School of Engineering, Tarbiat Modares University, Tehran, Iran*
[2]*Department of Information Technology, College of Engineering and Computer Science, Lebanese French University, Kurdistan Region, Iraq*
[3]*Department of Civil Engineering, College of Engineering, Salahaddin University-Erbil, 44002 Erbil, Kurdistan Region, Iraq*
[4]*Department of Computer Science, College of Science and Technology, University of Human Development, Sulaymaniyah, Kurdistan Region, Iraq*
[5]*Department of Communication and Computer Engineering, Faculty of Engineering, Cihan University-Erbil, Kurdistan Region, Iraq*

(*Received April 7, 2022, Revised June 27, 2022, Accepted August 14, 2022*)

Abstract. In this study, a Gaussian process regression (GPR) model as well as six GPR-based metaheuristic optimization models, including GPR-PSO, GPR-GWO, GPR-MVO, GPR-MFO, GPR-SCA, and GPR-SSO, were developed to predict fly-rock distance in the blasting operation of open pit mines. These models included GPR-SCA, GPR-SSO, GPR-MVO, and GPR. In the models that were obtained from the Soungun copper mine in Iran, a total of 300 datasets were used. These datasets included six input parameters and one output parameter (fly-rock). In order to conduct the assessment of the prediction outcomes, many statistical evaluation indices were used. In the end, it was determined that the performance prediction of the ML models to predict the fly-rock from high to low is GPR-PSO, GPR-GWO, GPR-MVO, GPR-MFO, GPR-SCA, GPR-SSO, and GPR with ranking scores of 66, 60, 54, 46, 43, 38, and 30 (for 5-fold method), respectively. These scores correspond in conclusion, the GPR-PSO model generated the most accurate findings, hence it was suggested that this model be used to forecast the fly-rock. In addition, the mutual information test, also known as MIT, was used in order to investigate the influence that each input parameter had on the fly-rock. In the end, it was determined that the stemming (T) parameter was the most effective of all the parameters on the fly-rock.

Keywords: fly-rock; hybrid models; machine learning; metaheuristic optimization; sensitivity analysis

1. Introduction

Demand for economic minerals has led to the rapid industrial expansion of mineral-based industries (Khandelwal and Monjezi 2013). Therefore, to close the gap between supply and demand, production from surface mines is increasing at a phenomenal rate. To date, drilling and blasting are weighed as the most cost-effective and efficient technique to excavation of rock masses from the earth's crust. After the blasting of a charged hole, a large amount of energy is released in the form of pressure, gas, heat, and stress waves. This blasting energy is not completely transformed into mechanical energy to split the rock mass into the desired size. Just 20% to 30% of this blasting energy is used for the real work, and the rest energy is wasted in the form of explosion disturbances such as back fractures, flying rocks, ground vibrations, noise, and air explosions (Peng *et al*. 2019). Among these explosion disturbances, fly-rock is considered as the main cause of financial and human losses related to surface mining (Fattahi and Hasanipanah 2021).

Fly-rock is an undesirable phenomenon in the operations of blasting, and is defined as pushing parts beyond a certain boundary which can lead to casualties, human injuries, and damage to structures. Both uncontrollable and controllable factors can affect the occurrence and severity of the fly-rock (Murlidhar *et al*. 2020). Controllable factors are changeable by blast charging, while uncontrollable factors are natural and unchangeable (Faradonbeh *et al*. 2018). The main controllable factors that cause the fly-rock phenomenon are insufficient load, improper latency, improper stemming, improper drilling, and unjustified powder factor (Khandelwal and Monjezi 2013). Also, factors such as poor geotechnical and geological conditions, especially the presence of loose strata of the rock in the upper part of the blast hole, are considered as the uncontrollable factors that affect the fly-rock distance (Kumar *et al*. 2021). Due to the involvement of different explosion design factors, the

*Corresponding author, Ph.D.
E-mail: h.nejati@modares.ac.ir
[a]M.Sc.
E-mail: m.arsalan@modares.ac.ir
[b]Ph.D.
E-mail: mukhtar@lfu.edu.krd
[c]M.Sc.
E-mail: hawkar.ibrahim@su.edu.krd
[d]M.Sc.
E-mail: shima.rashid@uhd.edu.iq
[e]M.Sc.
E-mail: adil.mohammed@cihanuniversity.edu.iq

ISSN: 2005-307X (Print), 2092-6219 (Online)

recommendation of specific methods for controlling and predicting the fly-rock is not easy (Harandizadeh and Jahed Armaghani 2021). Widely referred methods have been suggested, but subsequent studies have found deficiencies in these cases as well (Han *et al*. 2020, Hasanipanah *et al*. 2020, Ye *et al*. 2021).

Over the past few years, artificial intelligence (AI) and machine learning (ML) approaches such have shown a potential ability in the various civil, mining, and geo-engineering applications (Mahmoodzadeh *et al*. 2021a, Mahmoodzadeh *et al*. 2021b, Mahmoodzadeh *et al*. 2021c, Mahmoodzadeh *et al*. 2022, Xiang *et al*. 2021, Liu *et al*. 2021, Li *et al*. 2021, Bai *et al*. 2021). Also, several AI methods such as adaptive neuro fuzzy inference system (ANFIS), fuzzy inference system (FIS), support vector machine (SVM), conventional pattern recognition (CPR), extreme learning machine (ELM), gene expression programming (GEP), decision trees (DT), and artificial neural network (ANN) are applied by researchers to predict the fly-rock distance in the blasting operation and the potential ability of the AI methods in the prediction of fly-rock has been proved (Khandelwal and Monjezi 2013, Fattahi and Hasanipanah 2021, Faradonbeh *et al*. 2018, Kumar and Mishra 2021, Murlidhar *et al*. 2020, Guo *et al*. 2021a, Guo *et al*. 2021b). But some of these methods must be used when a lot of data are available. For example, CPR and ANN methods require sufficient number of data, which are sometimes not easy to obtain (Khandelwal and Monjezi 2013).

Given that we often face data shortages in geotechnical engineering issues, we need to use methods that have a high ability to solve problems with low data. Also, by optimizing these methods, models should be developed that give us the best performance in solving problems. The Gaussian process regression (GPR) method has shown a very good ability to solve various geotechnical problems with a small amount of data (Mahmoodzadeh *et al*. 2021a, Mahmoodzadeh *et al*. 2021b, Mahmoodzadeh *et al*. 2021c). The ability of the GPR method to predict the fly-rock distance has not yet been investigated. For this purpose, in this paper, the GPR method is used to predict the fly-rock in the blasting operations of open pit mines. In order to improve the GPR performance ability in the prediction of fly-rock, six hybrid models that are a combination of the GPR model and six metaheuristic optimization algorithms of grey wolf optimization (GWO), particle swarm optimization (PSO), social spider optimization (SSO), sine cosine algorithm (SCA), multiverse optimization (MVO), and moth flame optimization (MFO), are developed to fine-tuning of the GPR hyper-parameters.

300 datasets, including six input parameters of hole length (L), spacing (S), burden (B), stemming (T), powder factor (Pf), and sub-drilling (SD) and one output parameter (fly-rock) are utilized in the models obtained through the Soungun copper mine in Iran. Two cross validation methods of holdout and 5-fold are used to divide the datasets into two groups of training and testing. Several statistical evaluation indices are used to analyze the prediction results. Finally, comparing the prediction results made by the developed models with the measured fly-rocks, the most robust model is recommended. Also, the mutual information test (MIT) is used to examine the impact of each input parameter on the fly-rock.

2. ML methods

2.1 GPR

Gaussian process (GP) can be described as a non-parametric ML algorithm based on supervised learning, which is categorized into two kinds of classification and regression. While the target values of regression are continuous quantity predictions, the results of classification are discrete labels (Momeni *et al*. 2020). However, the definition of GP can be expressed as a set of arbitrary variables in which each limited subset of variables has a common multivariate Gaussian distribution. A GP is specified by the mean and covariance functions. Considering the mean function of $\mu(x)$ and the covariance function of $k(x,x')$, the $f\ (x)$ process can be defined as follows

$$\mu(x) = E\ [f(x)] \tag{1}$$

$$k(x,x') = E[\big(f(x) - \mu(x)\big)\big(f(x') - \mu(x')\big)] \tag{2}$$

Hence, the GP is defined as

$$f(X) \sim GP\big(\mu(X), k(X,X')\big) \tag{3}$$

For the simplicity of the notation, the function $\mu(x)$ is considered equal to zero. In addition, the function $\mu(x)$ will be computed using a function called the kernel function (Zhang and Xu 2020, Momeni *et al*. 2020).

For a real process of f, the training data are defined as

$$D = \left\{\left(X^{(i)}, y^{(y)}\right) \mid i = 1,2,\dots,n\right\} \tag{4}$$

where X is a dimension input vector, y is the corresponding true-valued noisy observation such that $y = f(X) + \in$, and n is the number of data.

Let D, X, and y considered as the collection of $d \times n$ (d is the dimension of matrix), input matrix, and target vectors, respectively. Now, D is defined as (Li *et al*. 2020)

$$D = \{X, y\} \tag{5}$$

Now, the challenge to calculation of the required values (f^*) for unknown input (X^*). As per the GP prior, the f and f^* joint distribution is (Li *et al* 2020)

$$\begin{bmatrix} f \\ f^* \end{bmatrix} \sim N\left(0, \begin{bmatrix} K + \sigma_n^2 I & K^{*^T} \\ K^* & K^{**} \end{bmatrix}\right) \tag{6}$$

where σ_n^2 is the noise variance, I is the Identity matrix, $K^*$is a matrix denoting the kernel function assessed for each member of $X^* \times X$ and similarly $K$is defined over $X \times X$ and K^{**}over $X^* \times X^*$.

Now, the conditional distribution of f^* given X^*, f and X can be found as (Mahmoodzadeh *et al*. 2021a)

$$f^*|X^*, X, f \sim N\left(K^*(K + \sigma_n^2 I)^{-1} f, K^{**} - K^*(K + \sigma_n^2 I)^{-1} K^{*^T}\right) \tag{7}$$

To reduction of the mean squared error, the best estimator of f^* is (Mahmoodzadeh *et al*. 2021b)

$$\hat{f}^* = K^*(K + \sigma_n^2 I)^{-1} f \quad (8)$$

The GP technique could be represented as the linear combination of n kernel functions (Deng *et al*. 2020).

$$\hat{f}^* = \sum_{i=1}^{n} \alpha^{(i)} k\left(x^*, x^{(i)}\right) \quad (9)$$

where α is the coefficient vector, and the optimal MSE coefficient vector will be $\alpha = (K + \sigma_n^2 I)^{-1} f$. Thus, the most crucial aspect of the GPR is the covariance (Kernel) function.

2.2 Metaheuristic optimization algorithms

2.2.1 Particle swarm optimization (PSO)

Kennedy and Eberhart established a swarm-based optimization technique called PSO (Kennedy and Eberhart 1995). This method searches the search space for the optimal answer using some particles (candidate solutions). Meanwhile, all of the particles are moving in the direction of the best particle (best solution) on their path. To put it another way, the particles regard their individual best solution as the best solution generally. To modify position in PSO, each particle needs to evaluate the current position, speed, distance to $pbest$, and distance to $gbest$ as Eqs. (10) and (11) (Kennedy and Eberhart 1995)

$$v_i^{t+1} = w v_i^t + c_1 \times \text{rand} \times (pbest_i - \chi_i^t) + c_2 \times \text{rand} \times (gbest - \chi_i^t) \quad (10)$$

$$\chi_i^{t+1} = \chi_i^t + v_i^{t+1} \quad (11)$$

where w represents a weighting coefficient, v_i^t denotes the i^{th} particle velocity at iteration t, x_i^t stands for the current position of particle i at iteration t, c_i is an acceleration factor, $rand$ stands for a random number in the range of (0,1]. Also, $gbest$ and $pbest_i$ are the best particle's position found so far and the best solution of particle i at iteration t, respectively.

2.2.2 Grey wolf optimization (GWO)

The GWO is a hunting-based optimization technique in which the best searching agent is considered alpha (α) to represent wolf hierarchical society mathematically. The following best solutions are beta (β) and delta (δ), and the remaining solutions are known as omega (ω). The optimization in GWO is directed by α, β and δ, and ω wolves belong to these mentioned categories. Eq. (12) is supplied to quantitatively illustrate the surrounding process (Mirjalili *et al*. 2014).

$$pos(t+1) = pos_p(t) - ac.pos_p(t) - pos(t) \quad (12)$$

where t denotes the current iteration, pos_p is the prey position, and $pos(t)$ is the candid solution's position. a and c vectors can be calculated using Eqs. (13) and (14), respectively (Taghavi and Khishe 2019).

$$a = 2.f.\text{rand}_1 - a \quad (13)$$

$$c = 2.\text{rand}_2 \quad (14)$$

where f decreases linearly from 2 to 0 during the iteration phase. $rand_1$ and $rand_2$ are random numbers in the range of [0,1]. First, GWO generates wolves at random. The wolves are then randomly assigned to one of three mentioned groups, each designated by a mathematical formula. The following equations represent the prey's drive:

Wolves can track and encircle their prey. Normally, α wolves perform the hunting process. Beta and delta wolves would help. Unfortunately, the search space lacks information on the prey (best solution). Mathematically, it is hypothesized that the α, β and δ wolves with the most knowledge about prey locations are the most experienced in the field. So, three of the best solutions are preserved, while other agents are forced to adjust their locations to match the best wolf's as following equations (Mirjalili *et al*. 2014)

$$pos(t+1) = \frac{pos_1 + pos_2 + pos_3}{3}, \quad pos_1 = pos_\alpha - a_1(d_\alpha), \; pos_2 = pos_\beta - a_2(d_\beta), \; pos_3 = pos_\delta - a_3(d_\delta) \quad (15)$$

$$d_\alpha = |c_1 pos_\alpha - pos|, \; d_\beta = |c_2 pos_\beta - pos|, \; d_\delta = |c_3 pos_\delta - pos| \quad (16)$$

2.2.3 Multiverse optimization (MVO)

The MVO is based on an evolving population of individuals. Each individual is a possible solution because its objects encode the three concepts of white, black, and wormholes. The multiple-candidate solutions collaborate and share information to move forward in promising directions. The best solution has a high probability of reproducing in order to guide space exploration toward promising solutions. As a result, the likelihood of falling into a local optimum is small (Mirjalili *et al*. 2016).

To integrate the solutions, random black and white holes are formed in universes, causing object movement. Furthermore, each universe has a fitness function, which is an inflation rate. MVO explores search spaces with white and black holes while exploiting them with wormholes. High-inflation universes always try to discard objects and transmit them to low-inflation realities. Also, low-inflation universes take stuff from high-inflation worlds to form a sustainable universe (i.e., state). After this method, all universes have equal inflation rates and are stable. During this step, the universes are established as normal, then arranged by inflation. At each step, wormhole tunnels sustain object interchange between local universes toward the best universe. This mechanism's model is as follows (Mirjalili *et al*. 2016)

$$Var_i^j = \begin{cases} \begin{cases} var_j + TDR \times rand_3 & (rand_4) < WEP \\ var_j - TDR \times rand_3 & (rand_4) < WEP \end{cases} & rand_5 < WEP \\ Var_i^j & rand_5 \geq WEP \end{cases} \quad (17)$$

where var_j denotes the j^{th} variable in the formed universe; Var_i^j denotes the j^{th} variable in the i^{th} universe; $rand_3$, $rand_4$, $rand_5$ denote random variables with values between 0 and 1; and the traveling distance rate (TDR) and wormhole existence probability (WEP) represent the two

significant coefficients, which are as follows (Mirjalili *et al*. 2016)

$$TDR = 1 - \left(\frac{t^{\frac{1}{accu}}}{T^{\frac{1}{accu}}} \right) \quad (18)$$

$$WEP = \min - t \times \left(\frac{\min - \max}{T} \right) \quad (19)$$

where $accu$ denotes the accuracy of exploitation over the iterations, min refers to the lower bound of WEP and, max refers to the upper bound of WEP, t indicates the current iteration, and T shows the maximum number of iterations.

2.2.4 Moth flame optimization (MFO)

Mirjalili (2015) created the MFO as a population-based metaheuristic algorithm inspired by the nighttime navigation strategy of moths. Moths and flames are the two primary components of MFO. In other population-based metaheuristics, moths stand in for the search agents or individuals. Depending on where the moth lands in the search area, we can infer a potential solution information about the problem. A position's length, then, represents the dimension of the problem to be optimized. P is a population of moths that may be modeled using Eq. (20) (Mirjalili 2015)

$$Posision = \begin{bmatrix} moth_{11} & moth_{12} & \cdots & moth_{1dim} \\ moth_{21} & moth_{22} & \cdots & moth_{2dim} \\ \vdots & \vdots & \vdots & \vdots \\ moth_{n1} & moth_{n2} & \cdots & moth_{ndim} \end{bmatrix} \quad (20)$$

There are n moths in the population, and dim is the total number of variables. A fitness function is used to determine each moth's fitness, and the results are stored in a matrix we'll call Outcome, as shown in Eq. (21) (Mirjalili 2015).

$$Outcome = \begin{bmatrix} Outmoth_1 \\ Outmoth_2 \\ \vdots \\ Outmoth_n \end{bmatrix} \quad (21)$$

$Outmoth_x$ is the $moth_x$'s fitness value. Flames are the second most important part of the MFO algorithm. The amount of moths inside the population determines the number of flames MFO maintains. Hence, they are expressed as a matrix of the same dimension as in Eq. (20). The flames' principal objective is to show each moth's best possible position. Similarly, to the population location in Eq. (21), the fitness of flames is stored in almost the same way. For moths, flames act as a memory; thus, each moth remembers the best position it has ever been in. MFO begins its iterative search procedure by producing a random population of moths based on these definitions. Finally, the moths are analyzed using a fitness function, and their performance is recorded as a series of flames. The moths' and flames' positions are constantly updated by MFO using a navigation technique. MFO uses the logarithmic spiral to determine the new location of each moth using Eq. (22) (Mirjalili 2015)

$$F\left(moth_i, flame_j\right) = D_{ij} e^{qt} \cos(2 \times \pi \times t) + flame_j \quad (22)$$

where, q denotes the logarithmic spiral shape, t denotes a random value in the range of $[r, 1]$ where r decreases from -1 to -2 during iterations, linearly. The distance between $moth_i$ and $flame_j$ is introduced by D_{ij} as shown in Eq. (23), in which the flame number decreases as Eq. (24) (Mirjalili 2015).

$$D_{ij} = \left| flame_j - fmoth_i \right| \quad (23)$$

$$flame_{No} = roind(\text{Max}(flame) - t \times \frac{Max(flame) - 1}{T} \quad (24)$$

where t *and* T denote the current and maximum number of iterations, respectively, and $\text{Max}(flame)$ is the maximum number of flames. where σ_θ is the tangential stress and q_c is the uniaxial crushistrength of the rock mass.

2.2.5 Sine cosine algorithm (SCA)

Mirjalili (2016) introduced a population-based optimization technique called SCA based on the trigonometry sine and cosine functions. The SCA updates the searching agents using Eq. (25) (Mirjalili 2016).

$$Loc_i^{t+1} = \begin{cases} Loc_i^t + rand_6 . \sin(rand_7) \times \\ |rand_8 . dest_i^t - Loc_i^t| \quad rand_9 < 0.5 \\ \\ Loc_i^t + rand_6 . \cos(rand_7) \times \\ |rand_8 . dest_i^t - Loc_i^t| \quad rand_9 \geq 0.5 \end{cases} \quad (25)$$

in which Loc_i^t and $dest_i^t$ are the location of the current response and the destination's location in the i^{th} dimension and t^{th} iteration. Also, $rand_6$ to $rand_9$ are random numbers in a range of $[0, 1]$. As illustrated in this equation, the algorithm has four major parameters, $rand_6$ to $rand_9$. The $rand_6$ the option specifies the next location region (or direction of travel) between the destination and source. The $rand_7$ the parameter specifies the movement distance away from the destination. The $rand_8$ variable specifies the size of the random weight used to reach the target (Mirjalili 2016). Finally, rand_9 alternates between sine and cosine components equally.

If rand_7 in Eq. (25) is specified as a random number in the range, the present mechanism ensures that the search region gets explored. A suitable algorithm will balance exploratory operations, identify potential search areas, and eventually converge to the real optimum. Eq. (26) adjusts the domain of the sine and cosine functions to maintain a balance between the exploration and exploitation phases.

$$r_1 = a - t\frac{a}{T} \quad (26)$$

where t and T are the current numbers, and the total number of iterations and a denotes a constant number. According to Mirjalili (2016), the algorithm will traverse the search apace when the cosine and sine amplitude are in the range $[-2, -1)$ and $(1,2]$. On the other hand, the algorithm converges to the optimum point between $[-1,1]$.

2.2.6 Social spider optimization (SSO)

The SSO considers the search space a shared spider web, with each possible solution representing a spider in the

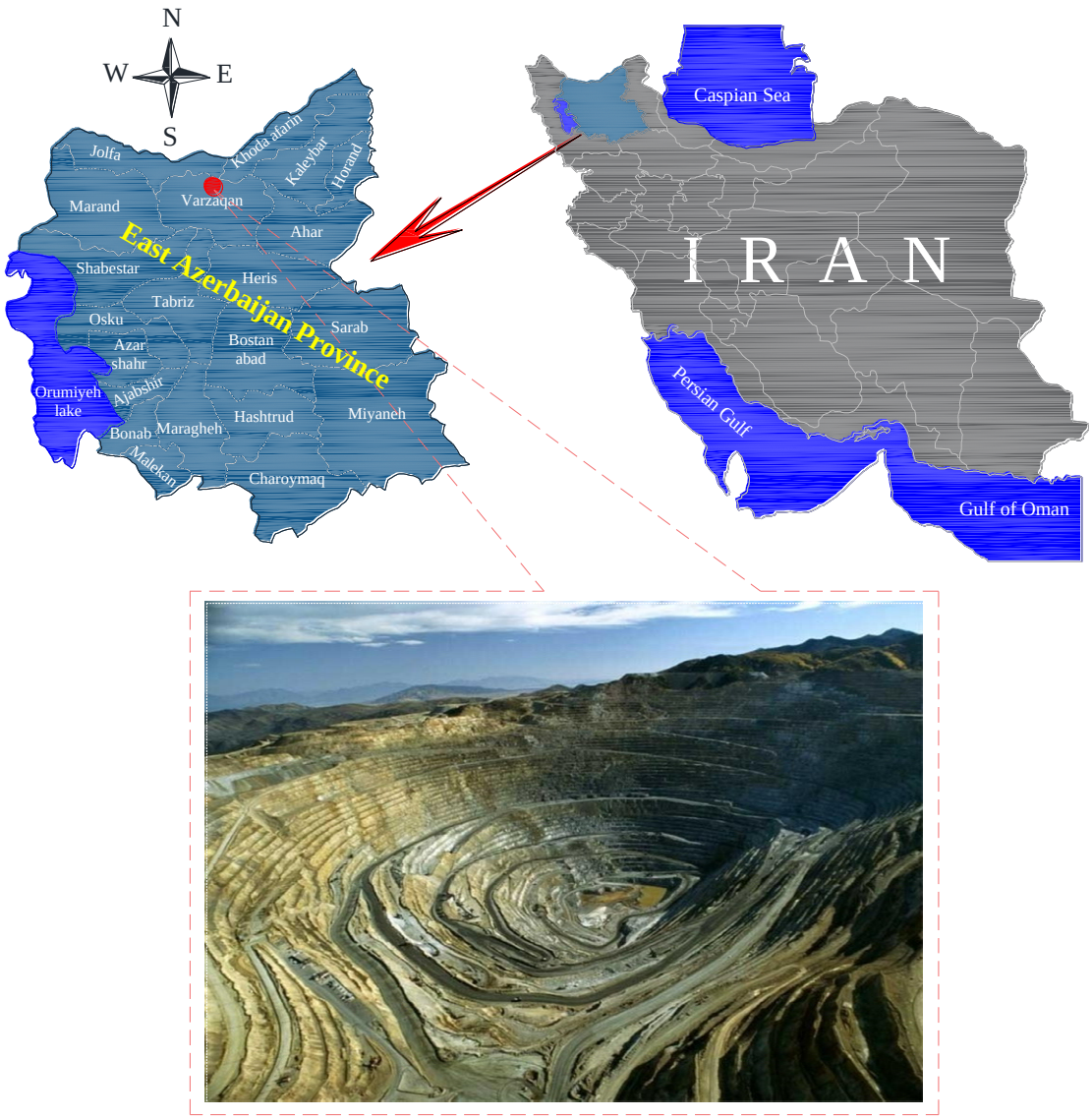

Fig. 1 Soungun copper mine location

population. Each spider is assigned a weight based on its fitness value in relation to the solution it means. The approach simulates two distinct sets of evolving controllers representing the colony's presumed cooperative behaviors (James and Li 2015). Each spider in SSO is assigned a weight $Wspider_j$ based on its solution fitness, which is determined as follows

$$Wspider_j = \frac{f(spider_j) - worst(spider)}{best(spider) - worst(spider)} \quad (27)$$

where $f(spider_j)$ denotes the j^{th} spider position's fitness value, $best(spider)$ and $worst(spider)$ denote the population's best and worst fitness values, respectively. The information exchange method is the primary mechanism through which the SSO optimizes the process. It is simulated by the web's vibrations. The vibration that a spider perceives is as follows (James and Li 2015)

$$\xi_{m,n} = Wspider_m e^{d_{m,n}^2} \quad (28)$$

where $Wspider_m$ denotes the j^{th} spider's weight and d denote the distance between the two spiders. Each spider can detect just three sorts of vibration: $vib_{i,m}$, $vib_{i,p}$, and $vib_{i,q}$. The new position $Fspider_i^k$ is obtained in the case of female spiders by changing the present spider position $Fspider_i^k$. The modification is determined at random by a probability factor P_f, and the movement is determined by the spider's proximity to other spiders and the vibrations conveyed across the search space (James and Li 2015)

$$Fspider_i^{k+1} = \begin{cases} Fspider_i^k + \beta vib_{i,m}.(spider_m - Fspider_i^k) + \\ \delta vib_{i,p}.(spider_p - Fspider_i^k) + \\ \eta\left(rand - \frac{1}{2}\right) with\ P_f \\ Fspider_i^k - \beta vib_{i,m}.(spider_m - Fspider_i^k) - \\ \delta vib_{i,p}.(spider_p - Fspider_i^k) + \\ \eta\left(rand - \frac{1}{2}\right) with\ 1 - P_f \end{cases} \quad (29)$$

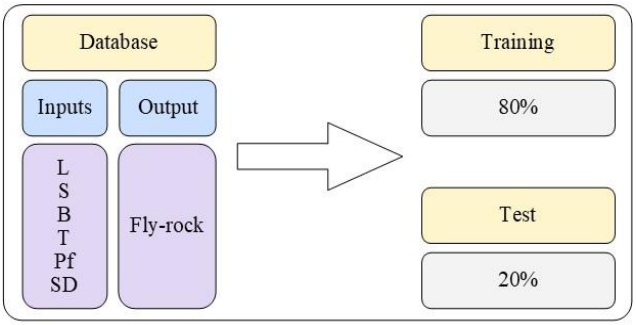

Fig. 2 Graphical explanation of the input and output variables used in this study

where, β, δ, and η and rand are random numbers between 0 and 1 and $spider_m$ represent the nearest spider with a weight greater than $Fspider_i^k$ and the best spider in the community web, respectively.

Male spiders, on the other hand, are classified into two groups: dominant (D) and non-dominant (ND). The group is integrated with the male spider, which has higher fitness values than the entire male set. Thus, the remainder of the male spiders constitutes the ND group. Male spiders are optimized using the following model (James and Li 2015)

$$mspider_i^{k+1} = \begin{cases} mspider_i^k + \beta vib_{i,m}.\left(spider_m - mspider_i^k\right) + \\ \qquad \eta\left(rand - \frac{1}{2}\right) \quad if \quad mspider_i^k \epsilon D \\ mspider_i^k + \beta.\left(\frac{\sum_{h\epsilon ND} mspider_h^k.Wspider_h}{\sum_{h\epsilon ND} Wspider_h} - mspider_i^k\right) \\ \qquad if \quad mspider_i^k \epsilon ND \end{cases} \quad (30)$$

Table 1 An overview of the database

Data		L	S	B	T	Pf	SD	Fly-rock
Training	count	240	240	240	240	240	240	240
	mean	12.2	4.1	3.3	2.9	0.7	0.8	49.9
	std	1.5	1.3	1.3	1.2	0.2	0.3	24.8
	min	10.0	2.0	1.2	1.1	0.2	0.3	10.8
	25%	11.0	2.9	2.1	1.9	0.5	0.5	31.8
	50%	12.1	3.9	3.1	2.8	0.7	0.8	35.2
	75%	13.5	4.9	4.1	3.7	0.8	1.1	70.0
	max	15.5	6.9	6.1	5.5	1.0	1.6	125.0
Testing	count	60	60	60	60	60	60	60
	mean	12.3	3.9	3.1	2.8	0.8	0.8	62.8
	std	1.5	1.3	1.3	1.2	0.2	0.3	24.8
	min	10.0	2.0	1.2	1.1	0.2	0.3	15.0
	25%	10.7	2.8	2.0	1.8	0.7	0.5	46.0
	50%	12.3	3.7	2.9	2.6	0.8	0.7	62.5
	75%	13.5	5.0	4.2	3.8	0.9	1.1	82.3
	max	15.1	6.8	6.0	5.4	1.0	1.5	125.0

3. Field study

Field survey was performed at Suongun copper mine, located 73 km northwest of Ahar in Azerbaijan province of Iran, at 46° 43' east longitude and 38° 42' north latitude at an altitude of 2000 meters above sea level. Hydrothermal infiltration is a dominant geological event in the Soungun mine, which has created a porphyry-type deposit. In this deposit, Sericite and Kaolinite, which are feldspar alteration products, are observable frequently. Mineralization is

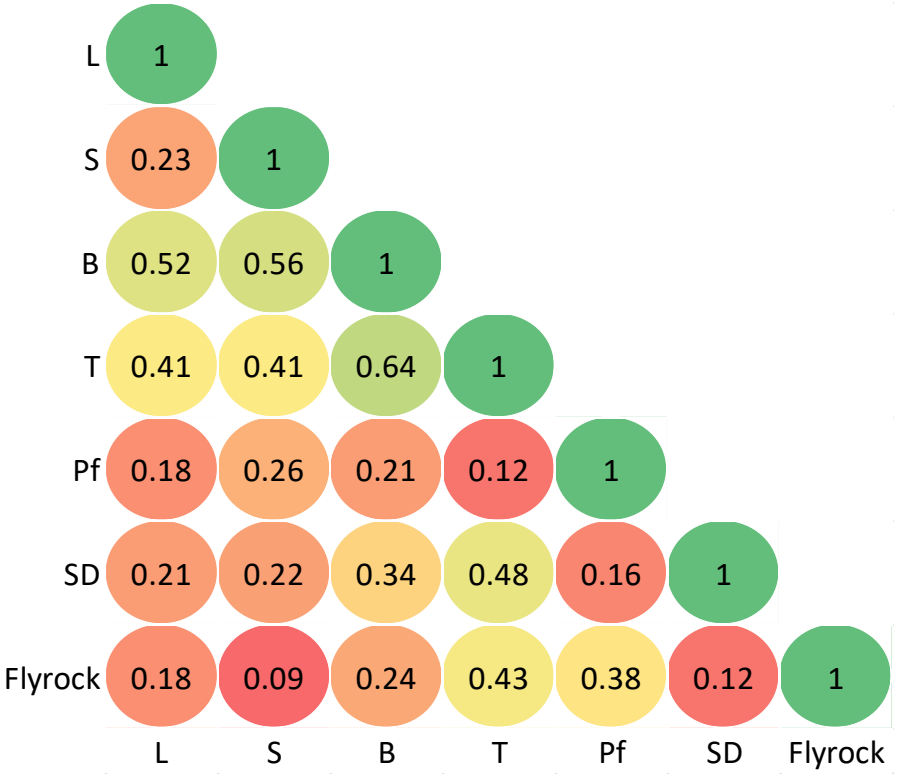

Fig. 3 The correlation matrix between the variables

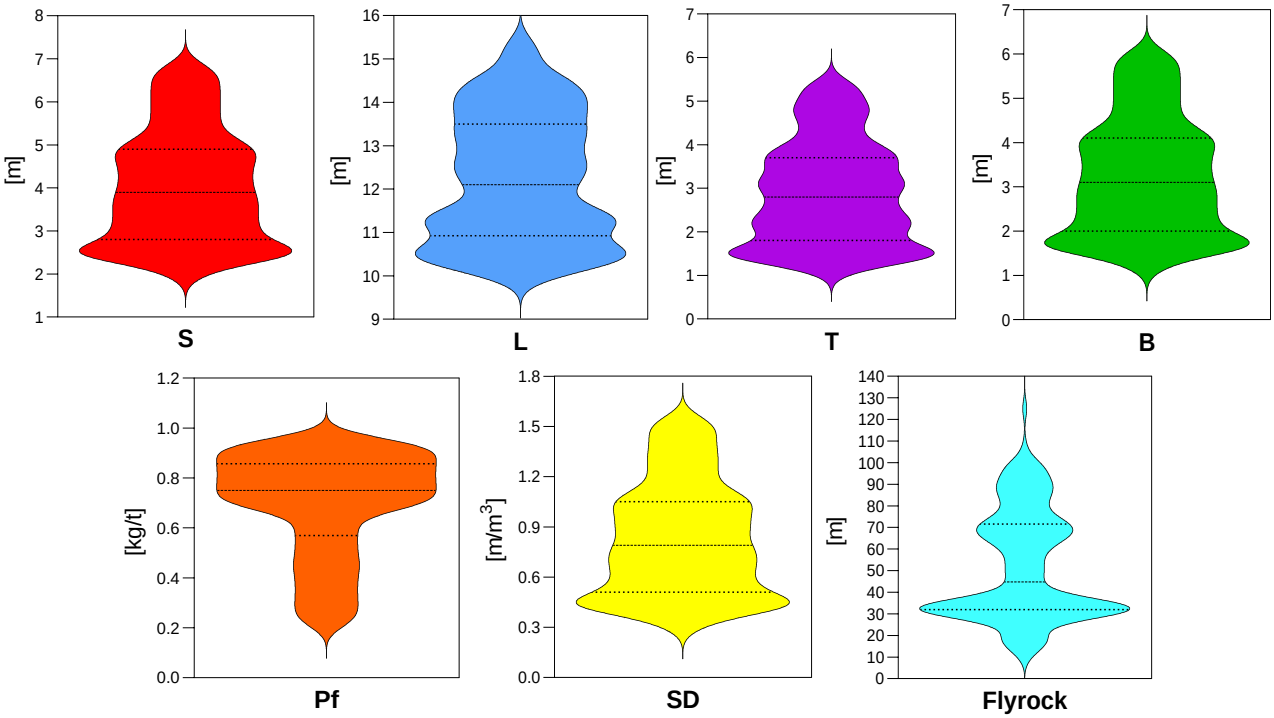

Fig. 4 The violin diagrams for each input and output

hosted mainly by modified rocks of Quartz-Monzonite. The silicification event along with the production of Quartz veins has caused the compaction of Porphyry rocks. Other minerals such as Molybdenite, Chalcopyrite, and Pyrite are also observed in the Soungun mine. The main and by-products elements of the Soungun mine are Copper and Molybdenum, respectively. For these products, there is usually a direct relationship between depth and degree, especially in the Hypogenic zone. The whole geological resources for this deposit are about 1000 million tons, while the proven reserves are about 388 million tons with an average grade of 0.67% Copper (Khandelwal and Monjezi 2013, Amini *et al*. 2012).

In the explosion operation of the Soungun mine, ANFO is used with an explosive rope, and drill cutting is used to stemming the explosion holes. The most crucial adverse events of the Songun mine explosion operation are fly-rock and backbreak. A maximum of 10 meters backbreak has been observed beyond the last row of explosion holes. Also, up to 100 meters of fly-rock has been observed in the blasting operation (Khandelwal and Monjezi 2013, Amini *et al*. 2012). The location and a view of the Songun copper mine is shown in Fig. 1.

4. Dataset preparation

In this work, 300 datasets were obtained in the Soungun copper mine. According to the literature (Kumar *et al*. 2021, Harandizadeh and Jahed Armaghani 2021, Han *et al*. 2020, Hasanipanah *et al*. 2020, Ye *et al*. 2021, Khandelwal and Monjezi 2013, Amini *et al*. 2012) and the data availability, six input parameters of hole length (L), spacing (S), burden (B), stemming (T), powder factor (Pf), and sub-drilling (SD) and one output parameter of fly-rock were considered in the database. 80% of datasets were applied for training and 20% for testing (Fig. 2). An overview on the database is presented in Table 1.

Fig. 3 presents the correlation matrix that exists between the six inputs and the output (fly-rock), which can be viewed in order to obtain additional information regarding the database. The correlations are evaluated using the Pearson correlation coefficient (R). R is an indicator to measure the linear correlation between two parameters, and the value of R can range from -1 to 1, which represents the greatest negative relationship all the way up to the greatest positive association.

Violin plots show the distribution of quantitative datasets at several levels of one or more classification variables. Fig. 4 shows the violin plots of the input and output parameters that were taken into account in this study.

The whole analysis and modeling procedure implemented by this work is summarized in Fig. 5. As can be seen from the figure, the methodology of this work is mainly includes four steps: (I) preparation of datasets, (II) establishment of model, (III) evaluation of the model, and (IV) analysis of the results. The hybrid models of GPR-PSO, GPR-GWO, GPR-MVO, GPR-MFO, GPR-SCA, and GPR-SSO are developed to fine tune the GPR hyper-parameters and then to improve the fly-rock predictions.

5. Statistical evaluation indices

To evaluate the accuracy of the forecasting models, some statistical evaluation indices, including coefficient of determination (R^2), root mean square error (RMSE), relative RMSE (RRMSE), mean absolute error (MAE),

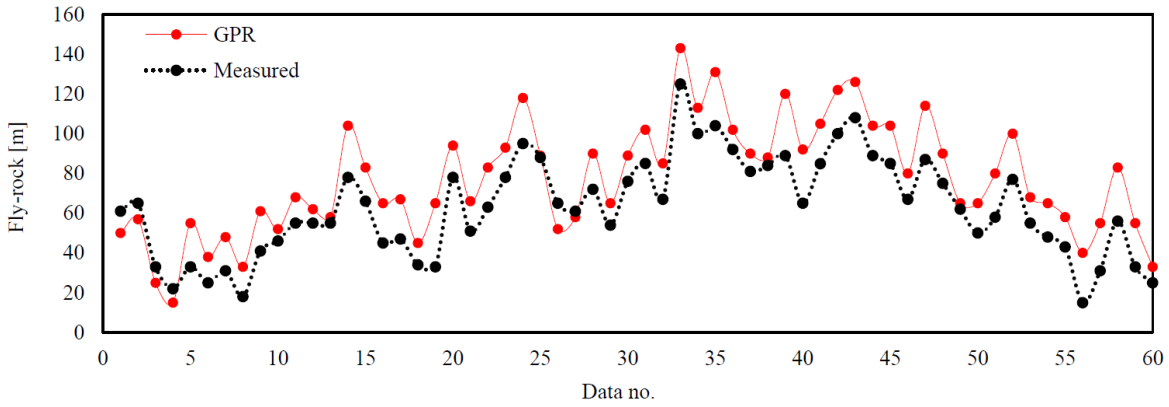

Fig. 6 Comparison of the GPR predictions with the measured fly-rocks

Table 2 The initial values of the hyper-parameters for the GPR model

Parameter	Value or type
KernelFunction (Form of the covariance function)	'Squared Exponential'
BasisFunction (Explicit basis in the GPR model)	'Constant'
Beta (Initial value of the coefficients for the explicit basis)	21.7096
Sigma (Initial value for the noise standard deviation of the Gaussian process model)	4.2506
FitMethod (Method to estimate parameters of the GPR model)	Exact Gaussian process regression

mean absolute percentage error (MAPE), and variance account for (VAF) are taken into account. The following formulas for calculating these indices are presented (Eqs. (31)-(36)).

$$R^2 = 1 - \frac{sum\ squared\ regression\ (SSR)}{sum\ of\ squares\ total\ (SST)} \quad (31)$$

$$\mathrm{MAE} = \left(\frac{1}{n}\right)\sum_{i=1}^{n}|y_i - y_i'| \quad (32)$$

$$\mathrm{MAPE} = \frac{1}{n}\sum_{i=1}^{n}\left|\frac{y_i - y_i'}{y_i}\right| \times 100\% \quad (33)$$

$$\mathrm{RMSE} = \sqrt{\left(\frac{1}{n}\right)\sum_{i=1}^{n}(y_i - y_i')^2} \quad (34)$$

$$\mathrm{RRMSE} = \sqrt{\left(\frac{1}{n}\right)\sum_{i=1}^{n}\left(\frac{y_i - y_i'}{y_i}\right)^2} \quad (35)$$

$$\mathrm{VAF} = 1 - \left[\frac{var(y_i - y_i')}{var(y_i)}\right] \times 100\% \quad (36)$$

where y_i is the actual value, y_i' is the predicted value, $\bar{y}_i$ and $\bar{y}_i'$ are the means of actual and predicted values, and n is the number of samples.

6. Results

6.1 Fly-rock prediction using GPR model

In the first step, the GPR model was ran without considering any approach to optimize its hyper-parameters. The initial hyper-parameters considered for the GPR model are presented in Table 2. The fly-rock values predicted by the GPR model for the testing datasets (20% of data) are shown in Fig. 6 and compared with the actual values. The evaluation statistical indices results for the GPR predictions are presented in Table 3. As it is clear from Fig. 6, for the most data points, about 20 meters or more errors are occurred in the prediction of fly-rock. Whether this amount of error is important in the designs or not, depends on the location of the explosion. For example, if the explosive location is close to engineering structures such as buildings or roads, this error rate is very important. Therefore, we should seek to propose a model that has the least errors and for different explosion situations, designs can be made based on it with more confidence. To this end, the GPR model should be optimized using different optimization algorithms to fine-tune its hyper-parameters. In the next step, six metaheuristic optimization algorithms are used for this purpose.

Table 3 Evaluation statistical indices results of the GPR model

MAE	RMSE	RRMSE	MAPE [%]	VAF	R^2
1.6	0.449	0.007	0.030	93.26	0.8693

6.2 Fly-rock prediction using GPR-based metaheuristic optimization algorithms

In this step, six metaheuristic optimization algorithms of PSO, GWO, MVO, MFO, SCA, and SSO are combined with the GPR model to make six hybrid models. The results of these hybrid models are compared with each other, and finally, the most robust model will be proposed. All the statistical evaluation indices results for the GPR model and the six hybrid models are presented in Table 4 for the training datasets. The R^2 value of the six mixed models is basically above 0.89, indicating that the six GPR-based metaheuristic optimization algorithms proposed in this study can achieve high training effects.

After the model training was completed, the testing datasets were utilized to verify and evaluate the hybrid models. The fly-rock predictions made by the GPR-PSO, GPR-GWO, GPR-MVO, GPR-MFO, GPR-SCA, and GPR-

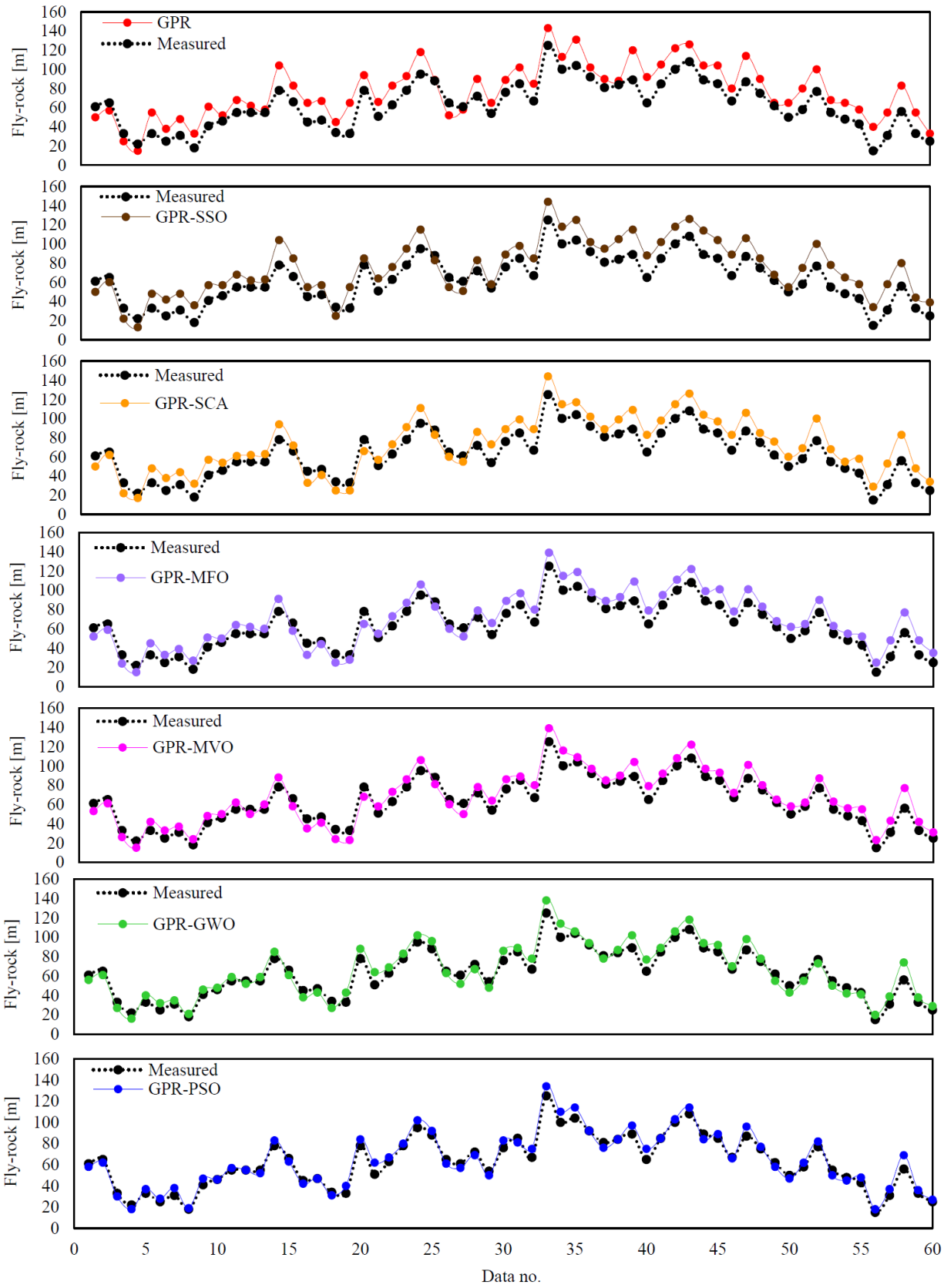

Fig. 7 Comparison of the measured fly-rocks and the fly-rocks predicted by the GPR and six hybrid models

SSO models are shown in Fig. 7 and compared with the measured mode individually. Looking at the diagrams provided in Fig. 7, the significant impact of the metaheuristic optimization algorithms can be seen on the GPR model performance. As can be seen, the difference between the predicted fly-rock values and the measured

Table 4 Comparison among the results produced by the GPR model and six hybrid models

	Method	R^2	Score	MAE	Score	RMSE	Score	RRMSE	Score	MAPE	Score	VAF	Score	Rank
Training	GPR	0.858	1	1.338	1	0.4312	1	0.0068	1	0.0280	1	94.119	1	6
	GPR-PSO	0.966	7	0.364	7	0.1039	7	0.0001	7	0.0067	7	99.153	7	42
	GPR-GWO	0.942	6	0.542	6	0.1852	6	0.0026	6	0.0089	6	98.812	6	36
	GPR-MVO	0.930	5	0.675	5	0.2306	5	0.0047	5	0.0145	5	98.642	5	30
	GPR-MFO	0.919	4	0.917	3	0.3081	4	0.0051	4	0.0158	4	98.413	4	23
	GPR-SCA	0.901	3	0.912	4	0.4102	2	0.0063	2	0.0239	3	97.186	3	17
	GPR-SSO	0.893	2	1.204	2	0.3827	3	0.0055	3	0.0264	2	96.720	2	14
Testing	GPR	0.869	1	1.602	1	0.4491	1	0.0074	1	0.0301	1	93.262	1	6
	GPR-PSO	0.967	7	0.443	7	0.1225	6	0.0020	5	0.0082	5	98.750	7	37
	GPR-GWO	0.947	6	0.635	6	0.2041	5	0.0033	4	0.0137	4	98.420	5	30
	GPR-MVO	0.928	5	0.844	5	0.3266	4	0.0054	3	0.0219	3	98.422	6	26
	GPR-MFO	0.917	4	1.010	4	0.3674	3	0.0060	2	0.0246	2	98.183	4	19
	GPR-SCA	0.894	3	1.264	3	0.4491	2	0.0074	1	0.0301	1	96.931	3	13
	GPR-SSO	0.883	2	1.515	2	0.4491	2	0.0074	1	0.0301	1	95.701	2	10

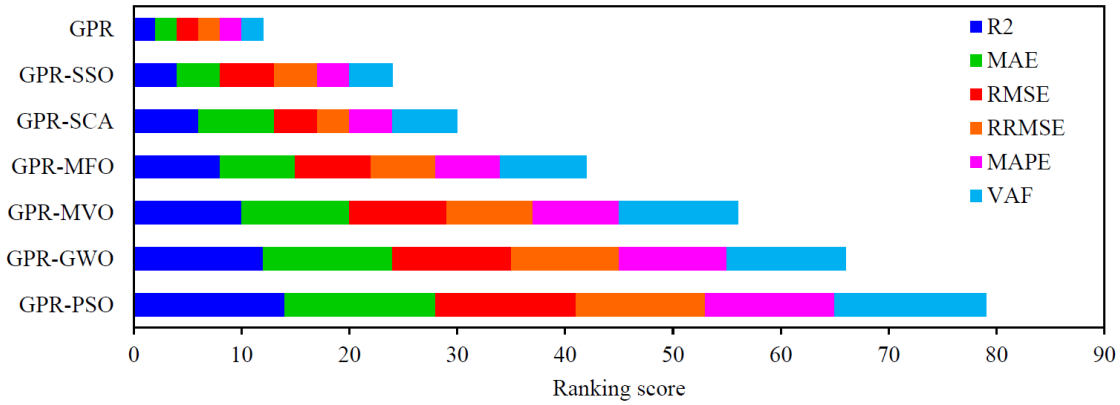

Fig. 8 The results of the overall ranking of training and testing

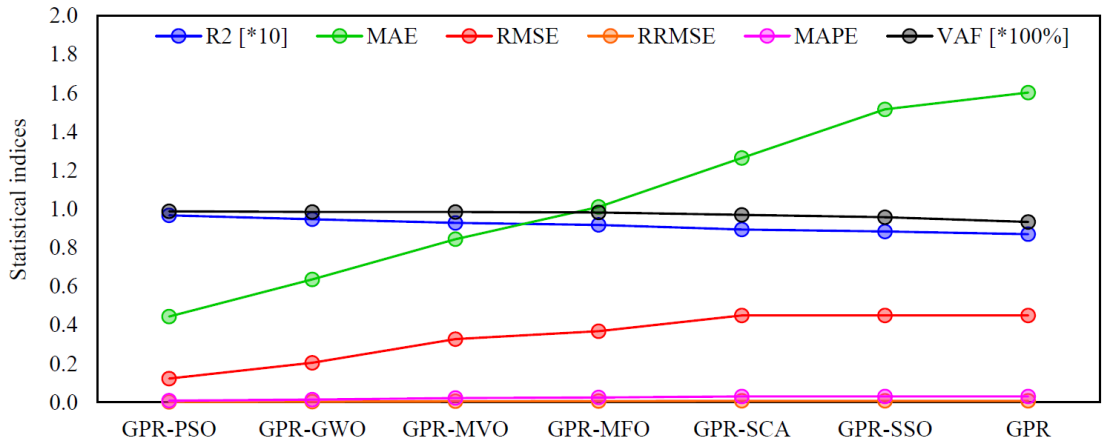

Fig. 9 The results of the evaluation indices of the testing

ones are decreased in all hybrid models, and the accuracy of the predictions is increased. The evaluation statistical indices results for the testing datasets are also presented in Table 4. As in Table 4, the prediction performance of the GPR model and the six hybrid models to predict the fly-rock from high to low is as follows:

GPR-PSO [MAE: 0.443; RMSE: 0.1225; RRMSE: 0.0020; MAPE: 0.0082; VAF: 98.750; R^2: 0.967]

GPR-GWO [MAE: 0.635; RMSE: 0.2041; RRMSE: 0.0033; MAPE: 0.0137; VAF: 98.420; R^2: 0.947]

GPR-MVO [MAE: 0.844; RMSE: 0.3266; RRMSE: 0.0054; MAPE: 0.0219; VAF: 98.422; R^2: 0.928]

GPR-MFO [MAE: 1.010; RMSE: 0.3674; RRMSE: 0.0060; MAPE: 0.0246; VAF: 98.183; R^2: 0.917]

GPR-SCA [MAE: 1.264; RMSE: 0.4491; RRMSE: 0.0074; MAPE: 0.0301; VAF: 96.931; R^2: 0.894]

GPR-SSO [MAE: 1.515; RMSE: 0.4491; RRMSE: 0.0074; MAPE: 0.0301; VAF: 95.701; R^2: 0.883]

GPR [MAE: 1.602; RMSE: 0.4491; RRMSE: 0.0074; MAPE: 0.0301; VAF: 93.262; R^2: 0.869]

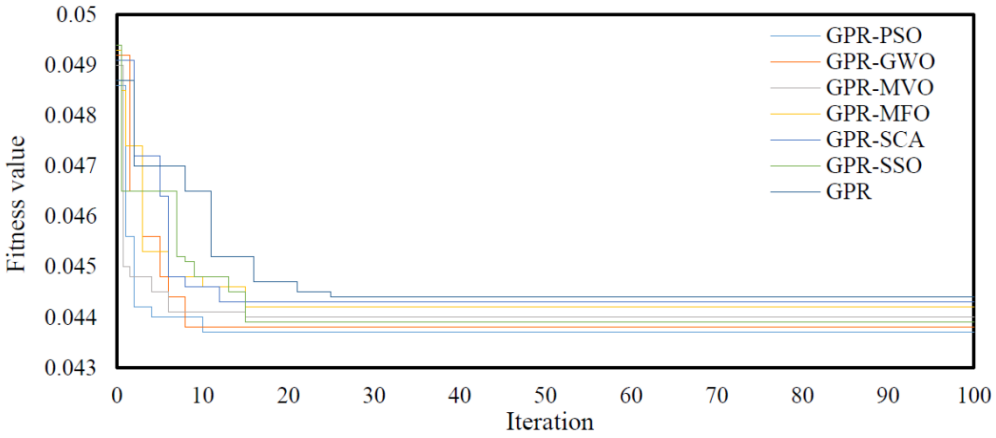

Fig. 10 The changes of fitness with iteration in the process of optimization

Table 5 Comparison among the 5-fold cross validation results produced by the applied ML models.

Method	R^2	Score	MAE	Score	RMSE	Score	RRMSE	Score	MAPE	Score	VAF	Score	Rank
GPR-PSO	0.962	11	0.478	11	0.1322	11	0.0028	11	0.0091	11	98.271	11	66
GPR-GWO	0.941	10	0.659	10	0.2167	10	0.0042	10	0.0119	10	97.401	10	60
GPR-MVO	0.930	9	0.833	9	0.3018	9	0.0051	9	0.0189	9	97.812	9	54
GPR-MFO	0.922	8	0.981	8	0.3498	8	0.0062	7	0.0255	8	97.593	7	46
GPR-SCA	0.902	7	1.213	6	0.4062	7	0.0058	8	0.0316	7	96.417	8	43
GPR-SSO	0.893	6	1.160	7	0.4813	6	0.0079	6	0.0325	6	95.509	7	38
GPR	0.874	5	1.558	5	0.5210	5	0.0085	5	0.0359	5	93.450	5	30

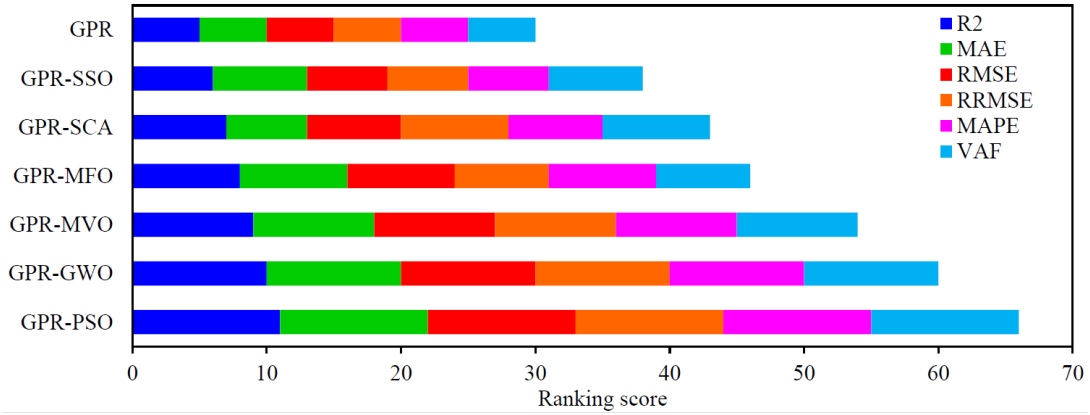

Fig. 11 The results of the overall ranking of 5-fold cross validation

These results indicate that the potential ability for all the six hybrid models to predict the fly-rock is high and more than the GPR model, but the GPR-PSO hybrid model has the best prediction performance.

To further analyze the results and compare the ML models' prediction performance, Table 4 also demonstrates the ranking system for each ML model of GPR-PSO, GPR-GWO, GPR-MVO, GPR-MFO, GPR-SCA, GPR-SSO, and GPR. Fig. 8 shows the results of the overall ranking in a more intuitive stacked graphs way. In Fig. 9, six statistical indices results for the GPR model and the six hybrid models are shown. The comprehensive results indicate that, the GPR-PSO hybrid model is the most robust and accurate model during training and testing compared to the other models. In addition, the GPR-PSO model features fast convergence speed, low error and high accuracy in the intelligent optimization process. The target optimization iteration diagram for the GPR and the six hybrid models is illustrated in Fig. 10. The good effect of the models can be seen, especially for the GPR-PSO model.

6.3 K-fold cross-validation

In the previous sections the holdout method was used to produce the results by the ML models, in which the database was divided into two parts of training (80%) and testing (20%). Now, the K-fold cross validation (K=5) method is used to include all the data used in this article in both training and testing data groups. This method is used to further analyze the results, avoid the over-fitting phenomenon (Liu *et al*. 2013), and to increase the level of confidence about the achieved performance of the models. The 5-fold cross-validation results in the prediction of fly-rock made by the seven ML models applied in this study,

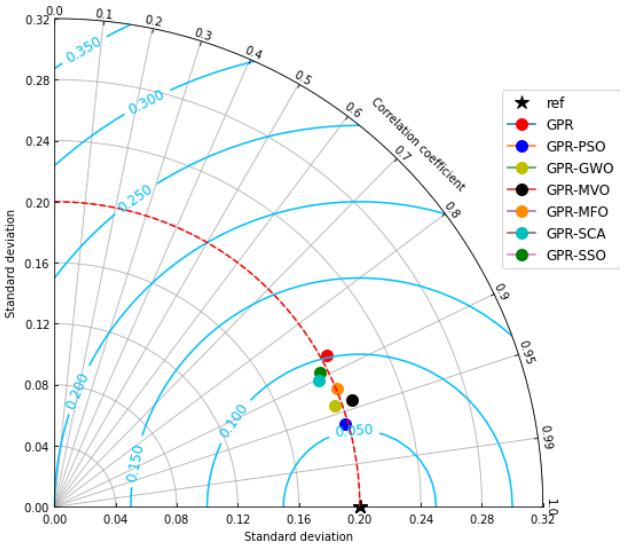

Fig. 12 Performance comparison according to the Taylor diagram for the 5-fold results

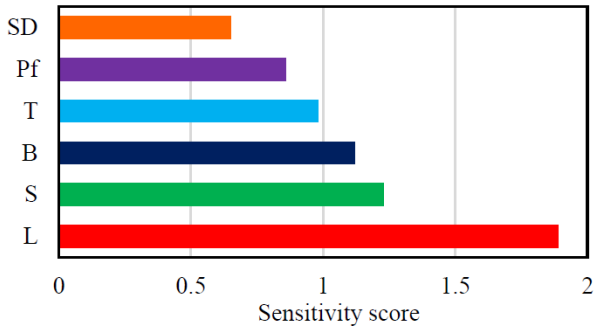

Fig. 13 Sensitivity score of the input parameters on the fly-rock

including GPR, GPR-PSO, GPR-GWO, GPR-MVO, GPR-MFO, GPR-SCA, and GPR-SSO are presented in Table 5. As presented in Table 5, the ranking scores achieved by the 5-fold cross-validation method follow the ranking scores achieved by the holdout method. The ranking score results for all the applied ML models are shown in Fig. 11. Also, the Taylor diagram obtained by the 5-fold cross-validation results is presented in Fig. 12. The analysis of these results concludes that the performance prediction of the ML models for both holdout and 5-fold methods from high to low are GPR-PSO, GPR-GWO, GPR-MVO, GPR-MFO, GPR-SCA, GPR-SSO, and GPR. Finally, this article recommends using the GPR-PSO hybrid model to predict the fly-rock in the blasting operation of open pit mines.

6.4 Parameters' sensitivity

To accurately estimate the fly-rock, the impact of each input parameter should be comprehensively studied and evaluated. In this study, six input parameters of L, B, S, T, Pf, and SD were taken into account as the effective parameters on the fly-rock. However, the sensitivity of these parameters individually is unclear on the fly-rock. For this purpose, the mutual information test (MIT) proposed by Verron *et al.* (2008) is used to examine the impact of each input parameter on the fly-rock. The MIT is a filtering technique applied to capture the desired relationship between each parameter and the label. This measure is the interdependence between parameters and shows the strength of the relationship between them. The information gain can calculate the mutual information size between the parameters (Eq. (37))

$$Gain(Y,X) = Ent(Y) - \sum_{v=1}^{V} \frac{|Y^v|}{|Y|} Ent(Y^v) \qquad (37)$$

where, v indicates the number of all possible values for X, Y^v is the set Y related to when x takes x_v, and Ent(Y) is the entropy of the information. As $Gain(Y,X)$ increases, the correlation between X and Y is increased.

Lastly, according to the score of the parameters in the MIT method, the importance degree of the input parameters on the fly-rock was calculated. The results obtained by the MIT method are illustrated in Fig. 13 for each input parameter. Looking at Fig. 13, it is revealed that all the six parameters of L, S, B, T, Pf, and SD with important scores of 1.89, 1.25, 1.12, 0.98, 0.86, and 0.65 greatly impact the fly-rock. Therefore, these parameters are influential parameters that need to be considered in predicting the fly-rock. It also should be noted that, among the six input parameters, L and SD have the most and least impact on the fly-rock, respectively.

7. Conclusions

In this work, six GPR-based metaheuristic optimization algorithms of GPR-PSO, GPR-GWO, GPR-MVO, GPR-MFO, GPR-SCA, and GPR-SSO were developed to predict the fly-rock in the blasting operation of open pit mines. 300 datasets were utilized in the models obtained from Soungun copper mine in Iran. To divide the database into two training and testing groups, two cross-validation methods of holdout and 5-fold were used. The ranking scores for each model evaluated using different statistical indices for both holdout and 5-fold methods indicated that the GPR model's accuracy to predict the fly-rock is not significant. But, a combination of GPR model and six metaheuristic optimization algorithms (GPR-PSO, GPR-GWO, GPR-MVO, GPR-MFO, GPR-SCA, GPR-SSO) led to fine-tune the hyper-parameters of the GPR model and finally to improve the fly-rock predictions, significantly.

In Fig. 14, to evaluate the developed models' performance, the statistical evaluation indicators are displayed through a recently proposed thermal map matrix called the accuracy matrix. Taking into account the ideal value as a reference, the accuracy obtained by the developed models for each performance index are calculated. For example, the ideal values for R^2 and VAF, MAE, and RMSE are 1, 100, 0 and 0, respectively. In this study, for the GPR-PSO model, these values were obtained by about 0.966, 99.153, 0.36 and 0.1039, respectively, in the training phase. Hence, the GPR-PSO model's accuracy is calculated as 97% (0.966/1 ≈ 0.97), 99% (99.153/100 ≈ 0.99), 64% (1-0.36=0.64) and 90% (1-0.1039≈0.90) respectively, in terms of R^2, VAF, MAE, and

RMSE. For the other indices in the all phases of training, testing, and 5-fold, the same procedure was followed. As in Fig. 14, the performance prediction of the models to predict the fly-rock for three phases of training, testing, and 5-fold from high to low are GPR-PSO, GPR-GWO, GPR-MVO, GPR-MFO, GPR-SCA, GPR-SSO, and GPR, respectively.

From these results it can be concluded that, the GPR model had not provided the acceptable accuracy. But all the six hybrid models offered better and more acceptable accuracies due to the optimization of their hyper-parameters. However, the accuracy of the GPR-PSO model was higher than all other models. Therefore, this article recommends using the GPR-PSO hybrid model to predict the fly-rock. By adopting this method, one can predict the fly-rock distance prior to blast and accordingly blast design can be modified to control and minimize the throw of fly-rock. Hence, blast nuisances can be minimized vis-à-vis more explosive energy can be utilized for the actual fragmentation and displacement of rock mass. Also, the input variables considered in this study, which are part of the controllable variables of fly-rock, in a way, they reflect the uncontrollable variables. For example, for unfavorable geological conditions that are part of the uncontrollable variables, lower values for parameters S and B of the blasting pattern are considered.

The MIT method was used in order to sensitivity analysis of the input parameters of L, S, B, T, Pf, and SD on the fly-rock. Finally, it was revealed that all the six input parameters of L, S, B, T, Pf, and SD with important scores of 1.89, 1.25, 1.12, 0.98, 0.86, and 0.65, respectively, significantly affect the fly-rock. However, parameter L and parameter SD were the most and least effective ones on the fly-rock, respectively.

References

Amini, H., Gholami, R., Monjezi, M., Torabi, S.R. and Zadhesh, J. (2012), "Evaluation of fly-rock phenomenon due to blasting operation by support vector machine", *Neur. Comput. Appl.*, **21**, 2077-2085. https://doi.org/10.1007/s00521-011-0631-5.

Bai, X., Cheng, W.C., Ong, D.E.L. and Li, G. (2021), "Evaluation of geological conditions and clogging of tunneling using machine learning", *Geomech. Eng.*, **25**(1), 59-73. https://doi.org/10.12989/gae.2021.25.1.059.

Deng, Z., Hu, X., Lin, X., Che, Y., Xu, L. and Guo, W. (2020), "Data-driven state of charge estimation for lithium-ion battery packs based on Gaussian process regression", *Energy*, **205**, 118000. https://doi.org/10.1016/j.energy.2020.118000.

Faradonbeh, R.S., Jahed Armaghani, D., Amnieh, H.B. and Mohamad, E.T. (2018), "Prediction and minimization of blast-induced fly-rock using gene expression programming and firefly algorithm", *Neur. Comput. Appl.*, **29**, 269-281. https://doi.org/10.1007/s00521-016-2537-8.

Fattahi, H. and Hasanipanah, M. (2021), "An integrated approach of ANFIS-grasshopper optimization algorithm to approximate fly-rock distance in mine blasting", *Eng. Comput*., **38**(3), 2619-2631. https://doi.org/10.1007/s00366-020-01231-4.

Guo, H., Nguyen, H., Bui, X.N. and Jahed Armaghani, D. (2021a), "A new technique to predict fly-rock in bench blasting based on an ensemble of support vector regression and GLMNET", *Eng. Comput.*, **37**, 421-435. https://doi.org/10.1007/s00366-019-00833-x.

Guo, H., Zhou, J., Koopialipoor, M., Jahed Armaghani, D. and Tahir, M.M. (2021b), "Deep neural network and whale optimization algorithm to assess flyrock induced by blasting", *Eng. Comput.*, **37**, 173-186. https://doi.org/10.1007/s00366-019-00816-y.

Han, H., Jahed Armaghani, D., Tarinejad, R., Zhou, J. and Tahir, M.M. (2020), "Random forest and bayesian network techniques for probabilistic prediction of fly-rock induced by blasting in quarry sites", *Nat. Resour. Res.*, **29**, 655-667. https://doi.org/10.1007/s11053-019-09611-4.

Harandizadeh, H. and Jahed Armaghani, D. (2021), "Prediction of air-overpressure induced by blasting using an ANFIS-PNN model optimized by GA", *Appl. Soft Comput.*, **99**, 106904. https://doi.org/10.1016/j.asoc.2020.106904.

Hasanipanah, M., Keshtegar, B., Thai, D.K. and Troung, N.T. (2020), "An ANN-adaptive dynamical harmony search algorithm to approximate the fly-rock resulting from blasting", *Eng. Comput.*, 1-13. https://doi.org/10.1007/s00366-020-01105-9.

James, J.Q. and Li, V.O.K. (2015), "A social spider algorithm for global optimization", *Appl. Soft Comput.*, **30**, 614-627. https://doi.org/10.1016/j.asoc.2015.02.014.

Kennedy, J. and Eberhart, R. (1995), "Particle swarm optimization", *Proceedings of ICNN'95-International Conference on Neural Networks*, **4**, 1942-1948, November.

Khandelwal, M. and Monjezi, M. (2013), "Prediction of fly-rock in open pit blasting operation using machine learning method", *Int. J. Min. Sci. Technol.*, **23**(3), 313-316. https://doi.org/10.1016/j.ijmst.2013.05.005.

Kumar, S., Mishra, A.K. and Choudhary, B.S. (2021), "Prediction of back break in blasting using random decision trees", *Eng. Comput.*, **38**(2), 1185-1191. https://doi.org/10.1007/s00366-020-01280-9.

Li, B., Fu, Y., Hong, Y. and Gao, Z (2021), "Deterministic and probabilistic analysis of tunnel face stability using support vector machine", *Geomech. Eng.*, **25**(1), 17-30. https://doi.org/10.12989/gae.2021.25.1.017.

Li, X., Yuan, C. and Wang, Z. (2020), "Multi-time-scale framework for prognostic health condition of lithium battery using modified Gaussian process regression and nonlinear regression", *J. Power Sour.*, **467**, 228358. https://doi.org/10.1016/j.jpowsour.2020.228358.

Liu, J., Jiang, Y., Zhang, Y. and Sakaguchi, O. (2021), "Influence of different combinations of measurement while drilling parameters by artificial neural network on estimation of tunnel support patterns", *Geomech. Eng.*, **25**(6), 439-454. https://doi.org/10.12989/gae.2021.25.6.439.

Liu, S., Tai, H., Ding, Q., Li, D., Xu, L. and Wei, Y. (2013), "A hybrid approach of support vector regression with genetic algorithm optimization for aquaculture water quality prediction", *Math. Comput. Model.*, **58**, 458-465. https://doi.org/10.1016/j.mcm.2011.11.021.

Mahmoodzadeh, A., Rashidi, S., Mohammed, A., Hama Ali, H. and Ibrahim, H. (2022), "Machine learning approaches to enable resource forecasting process of road tunnels construction", Communication Engineering and Computer Science, North America, March. Available at: <https://conferences.cihanuniversity.edu.iq/index.php/COCOS/22/paper/view/718>. Date accessed: 26 Sep. 2022.

Mahmoodzadeh, A., Mohammadi, M., Ibrahim, H.H., Abdulhamid, S.N., Ham-Ali, H.F., Hasan, A.M., Khishe, M. and Mahmud, H. (2021a), "Machine learning forecasting models of disc cutters life of tunnel boring machine", *Autom. Constr.*, **128**, 103779. https://doi.org/10.1016/j.autcon.2021.103779.

Mahmoodzadeh, A., Mohammadi, M., Ibrahim, H.H., Noori, K.M.G., Abdulhamid, S.N. and Hama-Ali, H.F. (2021c), "Forecasting sidewall displacement of underground caverns using machine learning techniques", *Autom. Constr.*, **123**, 103530. https://doi.org/10.1016/j.autcon.2020.103530.

Mahmoodzadeh, A., Mohammadi, M., Noori, K.M.G., Khishe, M., Ibrahim, H.H., Hama-Ali, H.F. and Abdulhamid, S.N. (2021b), "Presenting the best prediction model of water inflow into drill and blast tunnels among several machine learning techniques", *Autom. Constr.*, **127**, 103719. https://doi.org/10.1016/j.autcon.2021.103719.

Mirjalili, S. (2015), "Moth-flame optimization algorithm: A novel nature-inspired heuristic paradigm", *Knowled.-Bas. Syst.*, **89**, 228-249. https://doi.org/10.1016/j.knosys.2015.07.006.

Mirjalili, S. (2016), "SCA: A Sine Cosine Algorithm for solving optimization problems", *Knowled.-Bas. Syst.*, **96**, 120-133. https://doi.org/10.1016/j.knosys.2015.12.022.

Mirjalili, S., Mirjalili, S.M. and Hatamlou, A. (2016), "Multi-verse optimizer: A nature-inspired algorithm for global optimization", *Neur. Comput. Appl.*, **27**, 495-513. https://doi.org/10.1007/s00521-015-1870-7.

Mirjalili, S., Mirjalili, S.M. and Lewis, A. (2014), "Grey wolf optimizer", *Adv. Eng. Softw.*, **69**, 46-61 https://doi.org/10.1016/j.advengsoft.2013.12.007.

Momeni, E., Dowlatshahi, M.B., Omidinasab, F., Maizir, H. and Jahed Armaghani, D. (2020), "Gaussian process regression technique to estimate the pile bearing capacity", *Arab. J. Sci. Eng.*, **45**, 8255-8267. https://doi.org/10.1007/s13369-020-04683-4.

Murlidhar, B.R., Kumar, D., Jahed Armaghani, D., Mohamad, E.T., Roy, B. and Pham, B.T. (2020), "A Novel Intelligent ELM-BBO Technique for Predicting Distance of Mine Blasting-Induced Fly-rock", *Nat. Resour. Res.*, **29**, 4103-4120. https://doi.org/10.1007/s11053-020-09676-6.

Peng, Y., Su, Y., Wu, L. and Chen, C. (2019), "Study on the attenuation characteristics of seismic wave energy induced by underwater drilling and blasting", *Shock Vib.*, **2019**, Article ID 4367698. https://doi.org/10.1155/2019/4367698.

Taghavi, M. and Khishe, M. (2019), "A modified grey wolf optimizer by individual best memory and penalty factor for sonar and radar dataset classification", *Iran. J. Marine Technol.*, **6**(1), 122-132.

Verron, S., Tiplica, T. and Kobi, A. (2008), "Fault detection and identification with a new feature selection based on mutual information", *J. Proc. Control*, **18**, 479-490. https://doi.org/10.1016/j.jprocont.2007.08.003.

Xiang, G., Ying, D., Gao, C. and Yuan, L. (2021), "Application of artificial neural network for prediction of flow ability of soft soil subjected to vibrations", *Geomech. Eng.*, **25**(5), 395-403. https://doi.org/10.12989/gae.2021.25.5.395.

Ye, J., Koopialipoor, M., Zhou, J., Jahed Armaghani, D. and He, X. (2021), "A novel combination of tree-based modeling and monte carlo simulation for assessing risk levels of fly-rock induced by mine blasting", *Nat. Resour. Res.*, **30**, 225-243. https://doi.org/10.1007/s11053-020-09730-3.

Zhang, Y. and Xu, X. (2020), "Curie temperature modeling of magnetocaloric lanthanum manganites using Gaussian process regression", *J. Magnet. Magnetic Mater.*, **512**, 166998. https://doi.org/10.1016/j.jmmm.2020.166998.